




Analysis of the Integration of Aramid Fiber Tension Struts in a Box-shaped Pressure Vessel

Michael Ruf^{1,2}  · Alexander Hupfeld³ · Konstantin Heidacher³ · Dominik Joop³ · Christian Wrana³ · Alexander Horoschenkoff³

Received: 16 July 2021 / Accepted: 21 April 2022 / Published online: 23 May 2022
© The Author(s) 2022

Abstract

Shared vehicle architectures for fuel cell electric vehicles (FCEVs) and battery electric vehicles (BEVs) allow significant cost reduction in development and production by enabling economies of scale. Therefore, a box-shaped design for a type 4 pressure vessel is developed, which allows an efficient storage of hydrogen in conventional battery design spaces. For a load capable design, the top and bottom of the tank wall are connected with tension struts made of aramid fibers. Based on an analytical design, the geometry of the vessel is defined and a manufacturing process is developed using tufting as key technology for the insertion of the aramid fiber tension struts. The load transfer between the CFRP tank wall and the tension struts is crucial for the mechanical strength of the containment. Fiber loops are evaluated by guiding the tension struts through the CFRP tank wall and deflecting the load. In tensile tests, strengths of at least 1720 MPa are measured for this configuration. The tightness of the containment is ensured by a polymer liner and its adhesion to the struts. The interface between aramid fiber struts and the liner is investigated on strut-level analytically and in experiments. Different shear moduli of the investigated polymers show a major influence on the shear stress in the liner. For the application in the tension-braced pressure vessel, liner materials with the lowest possible modulus should be used to reduce the stress peaks in the liner. Finally, a design corridor for the dimensions of the tension struts and preferred material properties for the liner can be derived. For the investigated material, a strut diameter of 1 mm with a strut spacing of 3 to 5 mm is recommended.

Keywords Pressure Vessel · Hydrogen · Automotive · Aramid Fiber Strut · Fiber Loop

✉ Michael Ruf
michael.g.ruf@bmw.de

¹ Technical University of Munich, Boltzmannstraße 15, 85748 Garching, Germany

² BMW AG, Knorrstraße 147, 80798 Munich, Germany

³ University of Applied Sciences, Lothstraße 64, 80335 Munich, Germany

1 Introduction

Hydrogen is a noteworthy solution when it comes to an emission free mobility of the future [1]. In commercial and passenger vehicles it is used to run fuel cells and provide power for the electrical drivetrain. In current automotive applications gaseous hydrogen is stored in pressure vessels at 700 bar. Vehicles are equipped with one to three cylindrical containments with diameters larger than 200 mm to offer a sufficient cruising range [2, 3]. Type 4 pressure vessels represent the state-of-the-art and consist of a polymer liner which is wrapped in a carbon fiber reinforced plastic (CFRP) shell. While the liner is needed to keep the containment sealed and limit hydrogen permeation, CFRP is used to take up the load resulting from the inner pressure. Type 4 pressure vessels for hydrogen-fueled vehicles are generally designed according to Regulation No. 134 (R134) of the United Nations Economic Commission for Europe (UNECE) to fulfill safety-related requirements in operation [4].

Today battery electric vehicles (BEVs) are becoming more attractive for customers, while fuel cell electric vehicles (FCEVs) are still expensive as a result of cost-intensive development and manufacturing. Especially low production numbers as well as a dedicated vehicle architecture are cost drivers for the latter. Shared vehicle architectures for BEVs and FCEVs could enable economies of scale and significantly reduce costs for both vehicle concepts. This becomes possible by using similar design spaces for energy storage in both drivetrain variants. Therefore, hydrogen pressure vessels of FCEVs should be integrated in flat box-shaped design spaces in car underbodies, where BEVs are equipped with batteries.

The limited usable space for the integration of hydrogen containments requires an efficient storage concept to allow acceptable cruising ranges per tank of fuel. Several pressure vessel concepts for this application are shown in patent literature. They can be clustered in cylindrical approaches [5, 6] and cuboid designs with inner tension struts [7, 8]. Examples are shown in Fig. 1. Both concept variants have been investigated by Ruf et al. [9] regarding their potential storage volume. Although cylindrical containments cannot perfectly utilize the design space volume, they showed an acceptable possible storage volume for hydrogen to fulfill customer's expectations for cruising ranges. In comparison the box-shaped design offers a higher potential to increase the amount of storable fuel by 25% within the same design space.

Investigations on the design of cuboid pressure vessels with inner tension struts have been conducted by Oeztas et al. [11]. In their work, a fully metallic type I pressure vessel

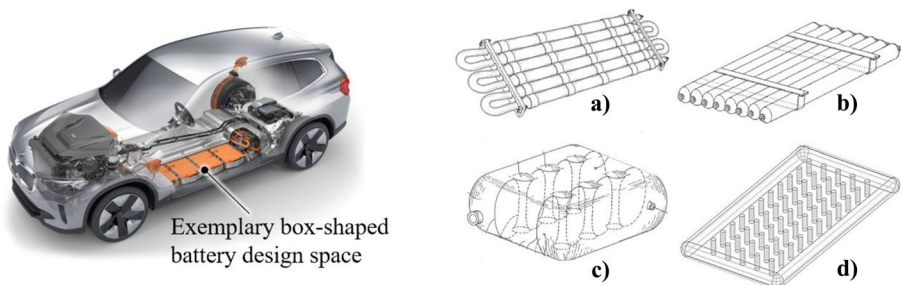


Fig. 1 Exemplary battery electric vehicle [10] (left) and pressure vessel solutions for box-shaped battery installation spaces (right): **a**) [5], **b**) [6], **c**) [7], **d**) [8]

was designed analytically and numerically and load conditions were assessed. As a result, an optimized design according to the minimum burst pressure of 157.5 MPa, determined in R134, was found through numerical simulations. A major disadvantage for Type I pressure vessels is the low gravimetric efficiency of the storage concept due to the low specific strength of the metal. In addition, especially for steel, hydrogen embrittlement can be critical for the safety of the vessel.

Therefore, a composite design has been proposed by Ruf et al. [9], Huber et al. [12] and Horoschenkoff et al. [13]. General strengthening possibilities of struts loaded in tension are discussed by Al-Mekhlafi et al. [14]. Furthermore, tethering possibilities of struts to planar surfaces are investigated in more detail by Khosravani et al. [15]. The investigated box-shaped pressure vessel in this work consists of a CFRP tank wall and is reinforced with aramid fiber tension struts. The tightness of the vessel is ensured by a polymer liner – a gas barrier on the inside of the CFRP tank wall. Based on a design concept, a manufacturing process was developed and validated using first prototypes. During pressure testing, the prototypes showed leakage at the corners from around 10 MPa.

This work focuses on the investigation of the adhesion between aramid fiber tension struts and the liner. The aim is to investigate factors that influence the design of a tension-strutted Type IV pressure vessel in order to permit the most efficient design possible. This concerns, on the one hand, the material selection for the liner as well as the struts and, on the other hand, the investigation of geometric quantities, such as the strut diameter and spacing as a function of strength. First, the structure of the vessel is introduced and based on analytical calculations the dimensions of the vessel parts are specified. In addition, the manufacturing process, which has a major influence on the design of the vessel, is briefly described. Subsequently, the mechanical adhesion between struts and tank wall is investigated in tensile tests. Analytical models and experiments are used to assess the tightness of the containment on coupon level. Finally, based on the results, an optimized design for a box-shaped vessel is derived.

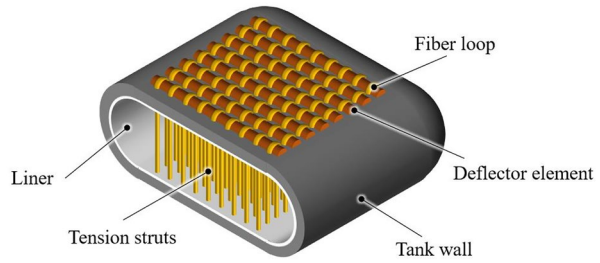
2 Pressure Vessel Concept

The investigated pressure vessel concept is designed for operation under a nominal working pressure (NWP) of 70 MPa. Safety-relevant aspects are derived from R134. To meet one of the main requirements, the burst pressure of the containment must exceed 225% of the NWP. This results in a design burst pressure of 157.5 MPa which determines the design of the investigated vessel.

2.1 Structure of the Pressure Vessel

In order to make optimum use of the flat box-shaped installation space, the pressure vessel should preferably have a cuboid shape. From a physical point of view, however, a spherical shape represents the optimum geometry for pressure vessels. Therefore, the cuboid containment is reinforced with an internal support structure for a pressure resistant design. Since the height of the design space is quite small compared to its width and length, tension struts are used to reinforce the top and bottom side of the vessel. The load transfer between struts and tank wall is ensured by a form closure of fiber loops. For this purpose, the struts penetrate the entire tank wall and are returned on the outside by a deflector element. The

Fig. 2 Cross section of the conceptual pressure vessel structure



corners and edges are replaced by quarter spheres and semi-cylinders to avoid high stress in the edges. An exemplary representation of the pressure vessel design is shown in Fig. 2.

2.2 Analytical Design Approach

The tank wall and tension struts of the pressure vessel are designed analytically according to [11]. The wall of the investigated vessel consists of CFRP having an orientation in circumferential direction in the semi-cylindrical areas and a 0° and 90° orientation in the plane areas. The thickness of the CFRP is determined by the semi-cylindrical areas. According to Barlow’s formula [16] the wall thickness $t_{0°/90°}$ is approximated by the tensile strength σ_{CFRP} , the radius r of the cylinder and the design burst pressure p :

$$t_{0°/90°} = \frac{p \cdot r}{\sigma_{CFRP}} \tag{1}$$

The size and number of the tension struts are estimated by an equilibrium of forces in one tension strut according to [11]. The relation between the strut spacing b , the diameter d of the tension struts, the design burst pressure p and the tensile strength σ_{strut} of the material used for the strut is determined according to formula 2:

$$b = \frac{d}{2} \cdot \sqrt{\pi \cdot \left(1 + \frac{\sigma_{strut}}{p} \right)} \tag{2}$$

Fig. 3 shows on the left the stresses acting in the container wall as a result of the internal pressure and on the right the stresses in the tension strut.

The wall thickness of the CFRP and the diameter and distance of the tension struts is determined according to the maximum allowable stress of the chosen material. The results

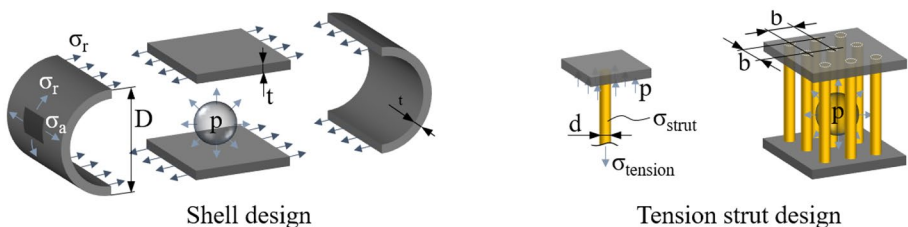


Fig. 3 Load condition in the pressure vessel according to [11]

of [11] have shown, that the analytical approach fits well, to design tank wall and tension struts according to the maximum allowable stress of the material.

The load deflection by fiber loops and the deflector elements results in an interlaminar shear loading on the CFRP tank wall which determines the maximum distance between the struts. The loads are shown in Fig. 4 on the basis of a strut deflection. To avoid damage to the CFRP wall during operation, the distance between the struts should not exceed 5 mm.

A strong interface between tension strut and liner is essential for the tightness of the containment. An effective adhesion between aramid fiber and liner material is a prerequisite for a strong interface. Within the investigated pressure vessel concept the liner is mainly pressure loaded – comparable to state-of-the-art pressure vessels with polymer liners. However, at the interphase area between tension strut and liner, the reacting force F of the tension strut faces the opposite direction of the internal pressure load p . Consequently, high shear loads are induced in the liner at this area and will be critical for the interphase. Shear stresses higher than 50 MPa might support crack formation in the interphase and should be avoided. Therefore, it is important to understand the factors influencing the shear stresses in the liner.

In [12] an analytical approximation of the critical shear stress within the interphase between fiber and liner is suggested. It is assumed, that the elongation of the tension strut induced by the pressure load is constant along the whole fiber. The resulting maximum shear stress $\tau_{Liner,max}$ of the liner varies depending on the distance x to the tension strut. It can be described as a function of the shear modulus G and the thickness t of the liner as well as the Young’s modulus E and the diameter d of the tension strut and the resulting force F :

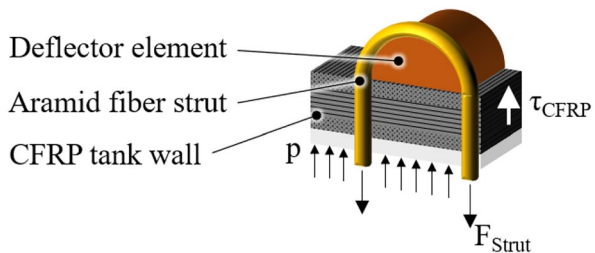
$$\tau_{Liner,max}(x) = \frac{G_{Liner} \cdot t_{Liner} \cdot F}{0.5 \cdot E_{strut} \cdot \pi \cdot d_{strut}^2 \cdot x} \tag{3}$$

The shear modulus G of the liner is determined as a function of the Young’s modulus E and the shear contraction coefficient ν [12]:

$$G_{Liner} = \frac{E_{Liner}}{2 \cdot (1 - \nu)} \tag{4}$$

A sensitivity study was performed in which x was varied from 0 to 2 mm and the Young’s modulus of the liner from 300 to 3000 MPa. The diameter of the tension strut is set at 1.3 mm. The reacting force F at the tension strut is derived from the internal pressure load as well as the geometrical design according to formula 2. The Young’s modulus of the strut is depending on the specific material. In the following, the behavior of the maximum shear stress of the liner is shown for a liner thickness of 5 mm and different moduli. The relationship between decay behavior and maximum shear stress is shown in Fig. 5.

Fig. 4 Resulting interlaminar shear stress τ_{ILS} in tank wall



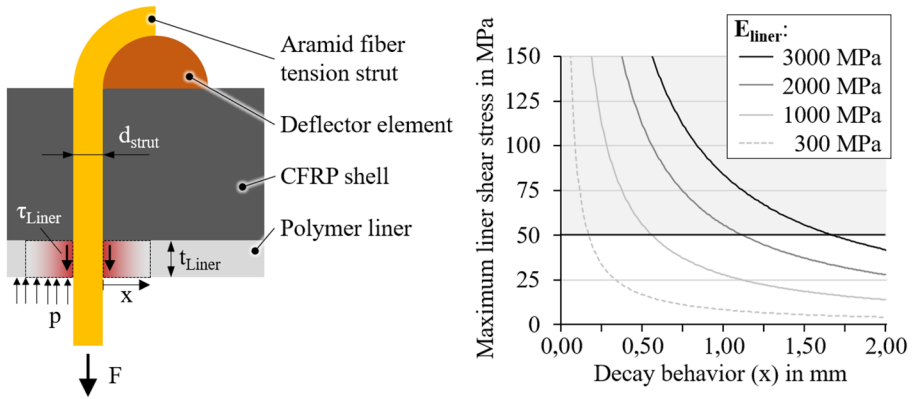


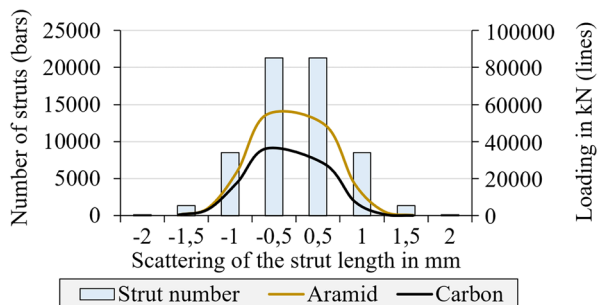
Fig. 5 Acting loads at the interphase between fiber and liner material (left) and influence of the decay behavior on the maximum shear stress of the liner for varying moduli of the liner (right)

The results show that materials with lower moduli lead to a significant reduction of the maximum shear stress of the liner. However, due to edge effects, the analytical approach is not suitable for determining the actual stresses of the liner near the tension struts. To show a more detailed stress distribution in the liner, numerical analyses are needed. These are addressed in the ongoing research, but not part of this paper.

2.3 Materials and Manufacturing Concept

FCEVs, which are based on a BEV architectures, require a storage-efficient containment design to fulfill customer’s cruising range expectations. State-of-the-art type 4 pressure vessels use carbon fiber reinforced composites to meet a minimum burst pressure of 157.5 MPa. For this reason, the tank wall of the investigated vessel is constructed from high-strength carbon fibers (Toray T700S). A stochastic analysis is performed for the material selection of the tension struts to study the influence of the strut length on the load carrying capacity of the vessel, since shorter struts will carry more load than longer struts. The load distribution was studied for carbon and aramid fibers for a normal distribution of the strut length referring to an average manufacturing tolerance of ± 0.5 mm. Figure 6 shows the strut loading for varying strut lengths due to manufacturing tolerances. Having

Fig. 6 Stochastic analysis of the load carrying capacity of different strut materials



a lower Young’s modulus aramid fibers can balance manufacturing tolerances better than carbon fibers.

Following the stochastic analysis and manufacturing concept, for the integration of the tension struts a material with high resistance to friction and high strength to low modulus ratio is needed. Thus, aramid fibers (Teijin D2200, 3220 dtex) are used for the tension struts. Thermoplastics (e.g. polyamide) or thermosets (e.g. epoxy resin) are considered for the liner and the loop deflector element on the outside of the vessel consists of a pressure-resistant metal.

The manufacturing process of the pressure vessel is shown in Fig. 7. It starts with a 3D-printed polymer core, which has the rough shape of the containment (step 1). In the next step, the carbon fibers are applied to the core in a filament winding process (step 2). Subsequently, dry aramid fibers are integrated using a tufting process (step 3). During tufting, the aramid fibers are guided in needles and penetrate the entire vessel from top to bottom (step 3.1). Since multi needle tufting is used as a process, at the bottom side the needle bar is pulled back slightly to form a fiber loop tunnel in the aramid fiber rovings (step 3.2). The metallic loop deflector is guided through the loop tunnel to fix the aramid fibers on the outside of the tank wall by form fit (step 3.3). Afterwards, the needles are retracted upwards again (step 3.4). On the top side another loop deflector is inserted and the needles are moved translational (step 3.5). This process is repeated for the entire plane area of the pressure vessel shell. After tufting, the carbon fibers are impregnated by resin transfer (step 4). To ensure that the inside of the container is not filled with matrix material during resin transfer molding, a concept with a lost core can be used. This core can, for example, consist of water-soluble or fusible material and be removed again after the RTM process. Finally, the core is removed and a polymer liner is formed through a roto molding process to keep the containment sealed against the environment (step 5).

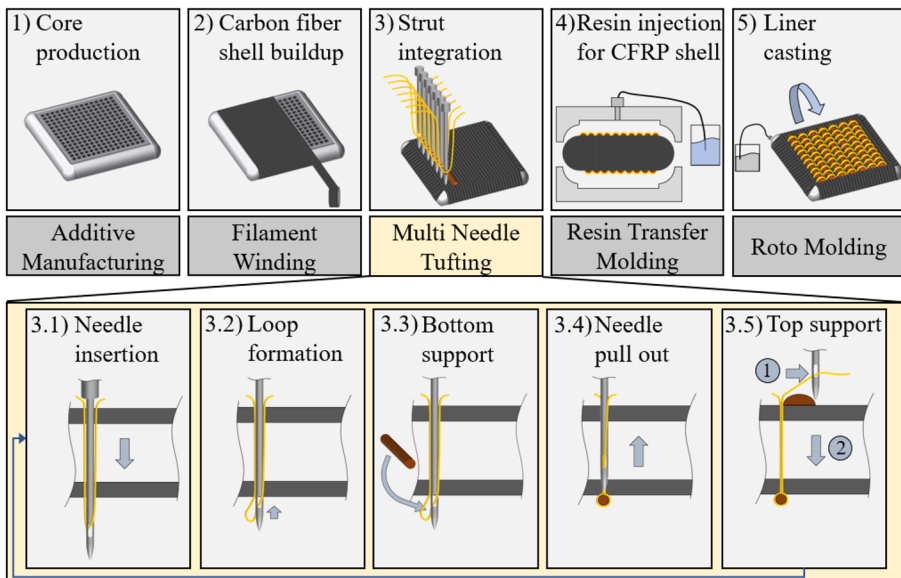


Fig. 7 Manufacturing process of the investigated pressure vessel concept based on [17]

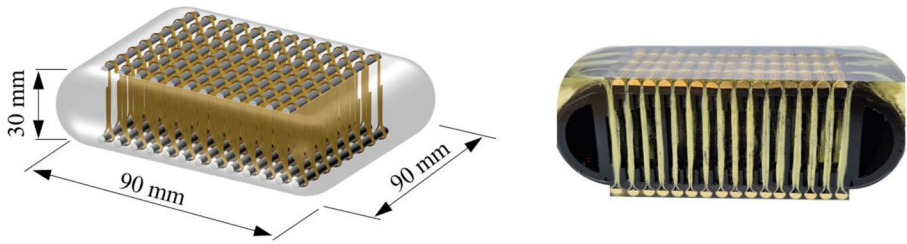


Fig. 8 Dimension of the investigated pressure vessel concept (left) and cross section of prototype without liner (right)

Based on the dimensions of a possible installation space in an FCEV, a subscale design for a prototype is developed. For the subscale prototype 256 tension struts with a diameter of roughly 1 mm and a spacing of 4 mm are used. The total containment length and width is 90 mm and the height is 30 mm. By building a prototype, the theoretical manufacturing concept without liner could be validated. The investigated vessel design is visualized in Fig. 8. The integration of a liner is under investigation.

3 Experimental Analysis

Subsequently, investigations are carried out to characterize the factors influencing the load transfer between fiber strut and CFRP tank wall. Furthermore, the adhesion between liner and strut is analyzed.

3.1 Investigation of the Fiber Loops

The load transfer between the aramid fiber tension struts and the CFRP tank wall is crucial for the mechanical design of the containment. The struts must carry the entire load in vertical direction. Therefore, it is decided to realize the strut connection via a form fit to enable a better load transfer into the the CFRP tank wall. According to the tufting process, two different fiber loops occur. A sewing stitch is used on the upper side and a tufting stitch on the

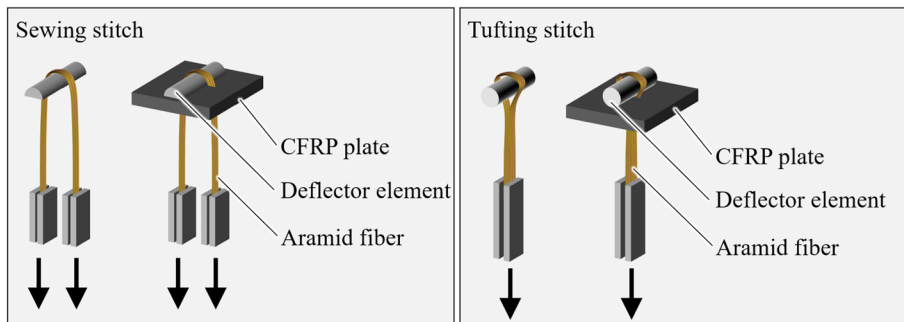


Fig. 9 Specimen types for tensile tests

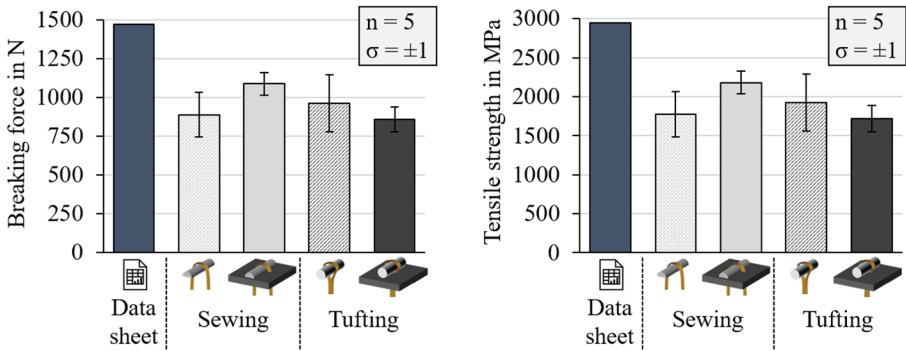


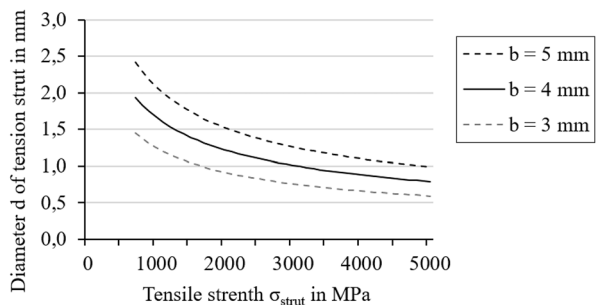
Fig. 10 Tensile test results for aramid fiber tension struts deflected by a support element

lower side. For both stitch types, tensile tests are conducted on strut level. The following test series consists of four different specimen types – two sewing and two tufting stitches each with and without CFRP plate. The test configurations are shown in Fig. 9. To enable a tufting stitch without a 10 mm thick CFRP plate, the aramid fiber ends are twisted before the tension test.

Within the experiment, the breaking force of the aramid fiber loops was measured. The results are shown in Fig. 10. A maximum breaking force of 1087 N is detected for a sewing stitch with CFRP plate. A tufting stitch with CFRP shows the minimum breaking force within the test series with a value of 858 N. Subsequently, the theoretical tensile strength of a tension strut is calculated. In order to do so, it is assumed that the aramid fiber filaments have the highest packaging density within the dry roving. This results in a minimum tensile strength of 1720 MPa for a tufting stitch with CFRP.

According to formula 2 the diameters of the tension struts depend on their spacing and tensile strength. In [12] a maximum distance of 3 to 5 mm between the struts is suggested to avoid high interlaminar shear stress in the CFRP tank wall. This opens a design corridor for a feasible strut design, which is shown in Fig. 11. In Sect. 2, a spacing of 4 mm was chosen for the subscale prototype. According to the minimum measured tensile strength, a theoretical strut diameter of 1.3 mm would be required to achieve a design burst pressure of 157.5 MPa:

Fig. 11 Diameter d of the tension struts depending on their spacing b and tensile strength σ_{strut} according to formula 2



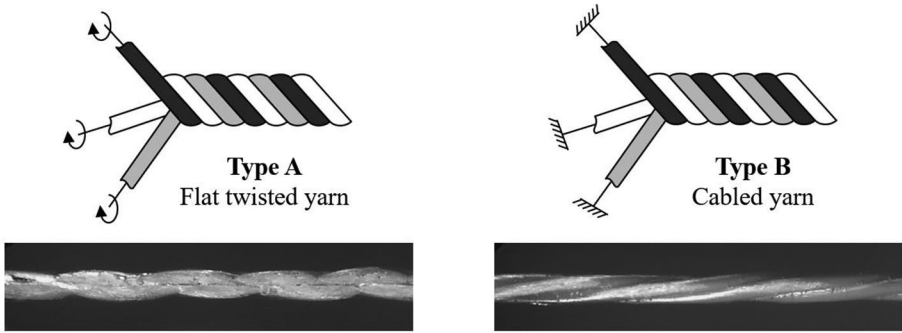


Fig. 12 Schematics of principal twisted yarn structures according to [18] (top) and microscope pictures of the tested yarns (below)

$$d = \frac{2 \cdot b}{\sqrt{\pi \cdot \left(1 + \frac{\sigma_{strut}}{p}\right)}} = \frac{2.4 \text{ mm}}{\sqrt{\pi \cdot \left(1 + \frac{1720 \text{ MPa}}{157.5 \text{ MPa}}\right)}} = 1.3 \text{ mm} \tag{15}$$

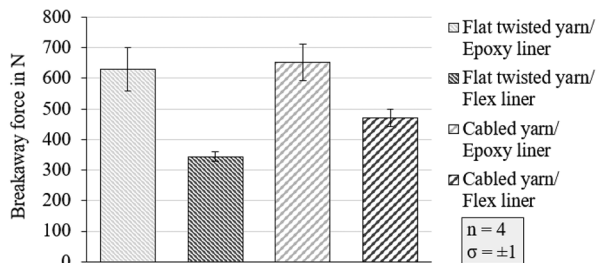
3.2 Investigations on the Interface Between Aramid Fiber Tension Strut and Liner

The analytical analysis has shown that lower Young’s moduli of the liner generally lead to lower shear stress in the liner. However, the effect on the adhesion between strut and liner cannot be assessed. Thus, experiments are carried out for further evaluation. Using pull-out tests the influence of material elasticity on the interface strength between liner and strut is investigated.

In the following experiment, two types of fiber yarns are used. Each of them consists of three aramid fiber rovings (Teijin D2200, 3220 dtex). Type A is a flat twisted yarn. In comparison to a single yarn, it shows better processability and fewer yarn faults as well as improved mechanical properties [18]. It is manufactured by first twisting the individual rovings and subsequently twist them around one another. Type B is a cabled yarn. In comparison to Type A it shows a lower risk of fiber damage during processing. Cabled yarns are manufactured by twisting the rovings around one another, without twisting the individual rovings [18]. Both fiber types are shown in Fig. 12.

Four different types of specimen are prepared for the test series. Flat twisted and cabled yarns are integrated in two types of epoxy resin plates with different Young’s moduli. Type

Fig. 13 Pull-out test results for cabled and twisted yarns from liner materials with different Young’s moduli



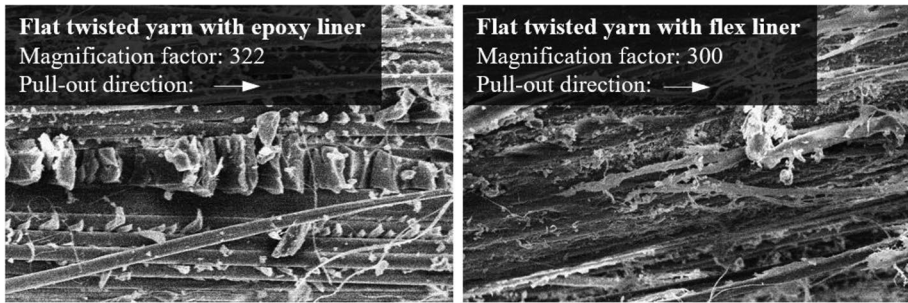


Fig. 14 Scanning electron analysis (SEM) to characterize the adhesion between aramid fiber and epoxy liner (left) as well as flex liner (right)

one of the investigated materials is an epoxy liner, which shows a Young's modulus of 3187 MPa after measurement. Type two is a flex liner, which consists of the epoxy liner and additional 30 weight-% of polyaminoamide for flexibilization. The flex liner shows a Young's modulus of 273 MPa after measurement. The plates have a length and width of 40 mm and a thickness of 5 mm. Tension tests in accordance to ISO 527 are conducted to determine the resulting Young's Modulus of the plate specimen [19].

In the pull-out test series, the breakaway force of the aramid fiber from the polymer is measured. The results are presented in Fig. 13 and show a similar adhesion strength for both yarn types with an epoxy liner. In comparison, a flex liner leads to a significantly lower breakaway force. This effect is stronger for flat twisted yarns than for cabled yarns. It is assumed, that different surface properties of the investigated yarn types have an influence on the breakaway force especially for liner materials with lower Young's moduli. Undercuts on the yarn surface might lead to a slight form fit in the liner and support the adhesion.

To evaluate the adhesion between liner and aramid fiber tension strut a scanning electron microscope (SEM) analysis is carried out for the flat twisted yarn type after the pull-out tests. Microscope images for both configurations are shown in Fig. 14. The yarn surface for the specimen with non-flexibilized epoxy liner shows "hackles", a characteristic for tough resin and shear failure which occurs due to tension strut pull-out [20]. In comparison, the second specimen with flex liner shows a ductile matrix behavior, the filaments show matrix particles indicating a strong interface for the flexibilized liner material.

4 Conclusions

The integration of aramid fiber tension struts in a box-shaped pressure vessel has been investigated. Based on previous studies, an analytical approach was applied to estimate the design and optimize the material selection of the pressure vessel. A stochastic investigation showed that the use of aramid fibers can balance manufacturing tolerances. The design of the tension struts was analyzed experimentally. The minimum measured tensile strength for the used material was 1720 MPa considering the loop design. Potential for higher tensile strength is seen by improved manufacturing quality of the strut deflection and advanced aramid fibers with higher strength. The research work aimed at a tensile strength higher than 2000 MPa and a strut diameter of about 1 mm to realize a strut spacing of 3 to 5 mm.

A sensitivity analysis was carried out analytically to determine the maximum shear stress of the liner. Due to the simplified analytical approach, the maximum values could not be calculated, which requires further numerical investigations. However, the results showed that the Young's modulus of the liner has a significant influence on the resulting shear stress. Lower liner moduli lead to a reduced stress pattern and shall be preferred for the application. The adhesion between aramid fiber tension strut and liner has been analyzed experimentally. For better processability during the tufting process, two different yarn types have been investigated. In combination with a softer liner, cabled yarns showed a higher breakaway force than flat twisted yarns. Thus, for further prototype series, aramid fiber tension struts shall be processed to cabled yarns – especially in combination with liner materials with a low modulus.

In further studies, numerical analyses should be performed to validate the analytical investigations. In particular, the decay behavior of the shear stress in the liner near the tension struts should be studied in more detail. Under pressure loading of the vessel, this is evaluated as particularly critical with regard to initial failure in the pressure vessel. Based on the numerical investigations, the vessel design can be further optimized and the theoretical investigations can be validated by experiments. Using burst tests, initial conclusions can be drawn on the tightness and load capacity of the pressure vessel design.

Acknowledgements The authors would like to express their gratitude to the German Federal Ministry for Economic Affairs and Energy for financial support within the government-funded national project “BRYSON”. Furthermore, the efforts of the editors and reviewers are gratefully acknowledged.

Author Contributions Michael Ruf: Methodology, Conceptualization, Writing – original draft, Writing – review & editing, Alexander Hupfeld: Methodology, Conceptualization, Konstantin Heidacher: Methodology, Conceptualization, Dominik Joop: Methodology, Christian Wrana: Methodology, Alexander Horoschenkoff: Methodology, Conceptualization, Resources, Project Administration, Validation, Supervision.

Funding Open Access funding enabled and organized by Projekt DEAL. The research was funded by the German Federal Ministry for Economic Affairs and Energy – funding code 03ETB019.

Data Availability The publication related datasets are available from the corresponding author on reasonable request.

Declarations

Ethics Approval and Consent to Participate Not applicable.

Adherence to National and International Regulations Not applicable.

Consent for Publication Not applicable.

Competing Interests The authors declare that they have no competing interests.

Open Access This article is licensed under a Creative Commons Attribution 4.0 International License, which permits use, sharing, adaptation, distribution and reproduction in any medium or format, as long as you give appropriate credit to the original author(s) and the source, provide a link to the Creative Commons licence, and indicate if changes were made. The images or other third party material in this article are included in the article's Creative Commons licence, unless indicated otherwise in a credit line to the material. If material is not included in the article's Creative Commons licence and your intended use is not permitted by statutory regulation or exceeds the permitted use, you will need to obtain permission directly from the copyright holder. To view a copy of this licence, visit <http://creativecommons.org/licenses/by/4.0/>.

References

1. Benitez, A., Wulf, C., de Palmenaer, A., Lengersdorf, M., Röding, T., Grube, T., Robinius, M., Stolten, D., Kuckshinrichs, W.: Ecological assessment of fuel cell electric vehicles with special focus on type IV carbon fiber hydrogen tank. *J. Clean. Prod.* **278**, 123277 (2021). <https://doi.org/10.1016/j.jclepro.2020.123277>
2. Klell, M., Eichlseder, H., Trattner, A.: *Wasserstoff in der Fahrzeugtechnik: Erzeugung, Speicherung, Anwendung*. Springer (2018). <https://doi.org/10.1007/978-3-658-20447-1>
3. Sasaki, K., Li, H., Hayashi, A., Yamabe, J., Ogura, T., Lyth, S.M.: *Hydrogen Energy Engineering: A Japanese Perspective*. Springer (2016). <https://doi.org/10.1007/978-4-431-56042-5>
4. Regulation No 134 of the Economic Commission for Europe of the United Nations (UN/ECE) – Uniform provisions concerning the approval of motor vehicles and their components with regard to the safety-related performance of hydrogen-fuelled vehicles (HFCV) [2019/795]. Official J European Union (2019)
5. Other Lab, L.L.C.: Tank enclosure and tank mount system method. US American patent application US **20180283610**, A1 (2018)
6. Kaisha, T.J.K.: Toyota-shi, Aichi-ken, JP: Hochdruckbehältereinheit. German patent application DE **102018116090**, A1 (2019)
7. Renault: Device for storing pressurised fluid and/or reactors generating pressurised fluids, in particular for motor vehicles. International patent application WO 0218836 A1 (2002)
8. Genesis, I.O.: LLC: Pressurized gas container and process. US American patent application US **20210080060**, A1 (2021)
9. Ruf, M., Stahl, H.-U., Kunze, K., Zarella, S., Horoschenkoff, A., Unwerth, T. v., Drechsler, K.: Neue Bauweisen von Wasserstoffdruckbehältern für die Integration in zukünftige Fahrzeugarchitekturen. Proceedings of the Munich Symposium on Lightweight Design 2020, Springer (2021). https://doi.org/10.1007/978-3-662-63143-0_8
10. BMW AG: The first-ever BMW iX3. Online press article. <https://www.press.bmwgroup.com/global/article/detail/T0310696EN/the-first-ever-bmw-ix3?language=en> (2020). Accessed July 5 2021
11. Öztas, K.A., Weerts, R.A.J., Ruf, M.G.: An analytical and numerical approach to design a type I box-shaped pressure vessel with inner tension struts. *Int. J. Press. Vessels Pip.* **192**, 104441 (2021). <https://doi.org/10.1016/j.ijpvp.2021.104441>
12. Huber, M., Hupfeld, A., Ruf, M., Horoschenkoff, A.: Bauraumoptimierter Wasserstofftank mit innerer Zugverstrebung. Proceedings of the Landshut Symposium on Lightweight Design 2021, LC-Verlag (2021). ISBN 978–3–9818439–5–8
13. A. Horoschenkoff, M. Huber, A. Hupfeld: Bauraumoptimierter Wasserstoff Tank mit innerer Zugverstrebung. Proceedings of the Munich Symposium on Lightweight Design 2020, Springer (2021). https://doi.org/10.1007/978-3-662-63143-0_9
14. Al-Mekhlafi, G.M., Al-Osta, M.A., Sharif, A.M.: Behavior of eccentrically loaded concrete-filled stainless steel tubular stub columns by CFRP composites. *Eng. Struct.* **205**, 110113 (2020). <https://doi.org/10.1016/j.engstruct.2019.110113>
15. Khosravani, M.R., Anders, D., Weinberg, K.: Influence of strain rate on fracture behavior of sandwich composite T-joints. *European Journal of Mechanics / A Solids* **78**, 103821 (2019). <https://doi.org/10.1016/j.euromechsol.2019.103821>
16. Grote, K.-H., Bender, B., Göhlich, D.: *Dubbel. Taschenbuch für den Maschinenbau*. Springer (2018). <https://doi.org/10.1007/978-3-662-54805-9>
17. BMW AG: Method for forming connections from a reinforcing fiber or reinforcing fibers, and method for producing a pressure container. International patent application WO **2021239565**, A1 (2021)
18. Cherif, C.: *Textile Material for Lightweight Constructions*. Springer (2016). <https://doi.org/10.1007/978-3-662-46341-3>
19. German Institute for Standardization (DIN): DIN EN ISO 527–4:1997, *Plastics - Determination of tensile properties - Part 4: Test conditions for isotropic and anisotropic fibre-reinforced plastic composites*, Beuth, Berlin (1997). <https://doi.org/10.31030/7360910>
20. Schmitt-Thomas, K.G.: *Integrierte Schadenanalyse*. Springer (2015). <https://doi.org/10.1007/978-3-662-46134-1>